Clean Techn Environ Policy (2014) 16:629–636
DOI 10.1007/s10098-013-0666-7

ORIGINAL PAPER

Modification of nano-TiO_2 by doping with nitrogen and fluorine and study acetaldehyde removal under visible light irradiation

Alireza Khalilzadeh · Shohreh Fatemi

Received: 24 February 2013 / Accepted: 29 July 2013 / Published online: 22 August 2013
© Springer-Verlag Berlin Heidelberg 2013

Abstract P25–TiO_2 nanoparticles were doped with fluorine, nitrogen, and their combination. Samples of N-doped, F-doped, and N–F-codoped TiO_2 were prepared by physical and chemical treatments. The products were characterized by X-ray diffraction, Fourier transform infrared, Brunauer–Emmett–Teller technique, and ultraviolet–visible diffuse reflectance spectroscopy. It was revealed that absorption spectra of N-doped, F-doped, and F–N-codoped TiO_2 were extended to the visible region wavelengths, and the photocatalytic experiments showed enhancement of acetaldehyde removal under visible light irradiation. The photocatalytic activity of the powders was evaluated through the process of acetaldehyde degradation under visible light scattering in a continuous stirred tank reactor. F–N-codoped nano-TiO_2 calcinated at 500 °C possessed the highest photocatalytic activity. The photocatalytic kinetic consumption of acetaldehyde was studied on N–F–TiO_2 powders under 80 W Hg lamp irradiation, and a Langmuir-type kinetic model was developed for the reaction with appropriate kinetic parameters.

Keywords TiO_2 nanoparticles · Visible light · Photocatalytic activity · F- and N-doped TiO_2 · Kinetic modeling · Acetaldehyde removal

A. Khalilzadeh · S. Fatemi (✉)
School of Chemical Engineering, University College of Engineering, University of Tehran, Enghelab Street, P.O. Box 11365-4563, Tehran, Iran
e-mail: shfatemi@ut.ac.ir

S. Fatemi
Oil and Gas Center of Excellence, School of Chemical Engineering, University of Tehran, Enghelab Street, P.O. Box 11365-4563, Tehran, Iran

Introduction

Photocatalytic technology is a promising and successful method among advanced oxidation processes, which can be used for degradation of environmental pollutants in air and water (Mills and Hunte 1997; Fujishima et al. 2000). TiO_2 is considered the most effective photocatalyst for its chemical stability, no toxicity, low cost, and environment-friendly feature (Mills and Hunte 1997; Fujishima et al. 2000; Linsebigler et al. 1995; Carey et al. 1976). However, application of TiO_2 is limited due to its wide band gap (3.2 eV), which requires ultraviolet (UV) irradiation for photocatalytic activation ($\lambda < 387$ nm) (Burda et al. 2003; Li et al. 2001). UV light accounts for only about 5 % of solar energy, while 45 % of its energy falls within visible light (Yin et al. 2003). Therefore, much attempt should be made for the enhancement of the photocatalysts under visible light scattering. One approach is the substitution of Ti atom by metals such as Fe, Mn, Au, Ag, and Cr (Klosek and Raftery 2001; Wu and Chen 2004). Also, photocatalytic activity of TiO_2 could be shifted to visible light by doping with nonmetal atoms, such as nitrogen, sulfur, carbon, and boron (Burda et al. 2003; Joung et al. 2006; Umebayashi et al. 2002; Le et al. 2012). The visible light photocatalysis of N-doped TiO_2 powders has been reported by many studies (Joung et al. 2006; Li et al. 2011).

It is accepted that N atoms can cause the redshift absorption threshold of TiO_2, but the doping mechanism is still under discussion. Most authors claim that substitutional N doped by O in anatase TiO_2 gives up narrowing of the band gap driven by mixing N 2p states with O 2p states (Asahi et al. 2001) and thus made it capable of absorbing visible light and representing visible activity. Irie et al. (2003) argued that the isolated narrow band placed above the valence band would be the reason for the visible response.

Fluorine doping in TiO_2 is also effective for enhancing the photocatalytic activity of TiO_2 (Yu et al. 2003; Hattori et al. 1999). Yu et al. (2003) found that F-doping can enhance surface area and crystalline structure of TiO_2. Also, they proposed that the doped F atoms converted Ti^{4+} to Ti^{3+} by charge compensation. A certain amount of Ti^{3+} reduced the rate of electron–hole recombination and consequently enhanced the photocatalytic activity. Hattori et al. (1999) approved that F-doping can improve the activity of TiO_2 according to the fact that doped F can increase the content of anatase. The F-doped TiO_2 also exhibited high activity due to improvement in surface acidic sites (Hattori et al. 1999), which would increase the reactant adsorptivity and also inhibit the recombination between electrons and holes.

Due to the synergetic promoting effects from the N and F dopants, F–N-codoped TiO_2 revealed very high activity in photocatalytic degradation of acetaldehyde under visible light irradiation (Li et al. 2005a, b).

In the present study, an accurately comparative study was carried out on the N-doped, F-doped, and F–N-codoped TiO_2 photocatalysts in the continuous mixed reactor. N-doped TiO_2 was prepared by annealing P25–TiO_2 in NH_4OH/N_2 flow at different temperatures. F-doped TiO_2 was synthesized from P25–TiO_2 by impregnation method, and F–N-codoped TiO_2 was prepared by the sol–gel method. The photocatalytic application of the prepared materials was investigated and kinetically modeled.

For the large-scale application of organic removal under visible light scattering, it is necessary to work in the open systems. Up to now, most of the studies have focused on the batch processes and UV irradiation, whereas in this study attempts are made for the preparation of the improved material and its application in continuous reactor to have a proper insight into the real conditions.

Experimental

Materials

Titanium dioxide (P25) was purchased from Sigma-Aldrich Chemical Company, and titanium tetraisopropoxide (TTIP) ($Ti(i\text{-}C_3H_7O_2)_4$, Panreac, 97 % pure), acetaldehyde (CH_3CHO, Merck, 99 % pure), ammonium fluoride (NH_4F, Merck), ammonium hydroxide 25 % (NH_4OH, Merck), and absolute ethanol (Merck) were prepared and used with no further treatment.

Synthesis

N-doped TiO_2 was prepared by thermal treatment method. First, the carrier gas (N_2) with flow rates of 5, 10, and 15 (N ml min^{-1}) was passed from a gas-washing bottle containing ammonium hydroxide. N-doped TiO_2 was prepared by thermal treatment of commercial P25–TiO_2 in NH_4OH/N_2 flow at 400, 500, and 600 °C for 3 h, which was carried out in a tubular furnace.

F-doped TiO_2 was synthesized from P25 to TiO_2 by impregnation method. TiO_2 powder was added into the mixture of NH_4F and a solution of ethanol in water starting with different mass ratios of 0.2, 0.3, and 0.4 NH_4F/TiO_2, stirred for 24 h at 40 °C, aged for 16 h at room temperature, and then dried at 80 °C for 8 h. The obtained powder was calcined at 400, 500, and 600 °C for 3 h.

The two-level factorial design with a center point was used to prepare the F- and N-doped samples. The experimental design with five tests for the preparation of F-doped and five tests for the preparation of N-doped samples was randomly implemented. The experimental conditions for the preparation of N- and F-doped samples are given in Table 1.

For preparing the N–F-codoped TiO_2, a sol–gel method was implemented; 0.3 g of NH_4F and 8 ml of NH_4OH (25 %) were added into a solution of ethanol in water (1:5 v/v) under vigorous stirring at room temperature. Then 3 ml of TTIP was added dropwise to the solution. The final solution was stirred for 24 h at 40 °C and aged for 16 h at room temperature. The solution was dried in an oven at 80 °C for 8 h to remove the water and then calcined at 500 °C for 3 h in a furnace.

Characterization techniques

The X-ray diffraction (XRD) patterns of the samples were measured with a Siemens D5000 diffractometer using Cu Kα radiation in angular domain of $10 < 2\theta < 80$ and $\lambda = 0.15406$ nm. For Fourier transform infrared (FT-IR) experiments, FT-IR spectrophotometer Thermo Nicolet

Table 1 Experimental conditions for the preparation of N- and F-doped samples

Run order	Samples	Calcination temperature (°C)	Flow rate carrier gas (N ml min^{-1})	NH_4F/TiO_2 (wt%)
1	N1	600	5	–
2	N2	500	10	–
3	N3	600	15	–
4	N4	400	5	–
5	N5	400	15	–
1	F1	400	–	0.2
2	F2	500	–	0.3
3	F3	400	–	0.4
4	F4	600	–	0.4
5	F5	600	–	0.2

was used. The samples were incorporated in KBr pellets, and IR spectra of the prepared samples were measured. The specific surface areas of the samples were determined by N_2 gas adsorption using a Brunauer–Emmett–Teller (BET) technique (Belsorp mini-II). The diffuse reflectance spectra (DRS) were obtained to measure the absorbance data of the samples using a UV–Vis spectrophotometer (model Avaspec-2048-TEC), and $BaSO_4$ was used as a reference.

Photocatalytic activity test

The photocatalytic experiments were performed in a 198-ml continuous stirred laboratory-scale reactor, equipped with a quartz head. The reactor was placed in the dark woody box. The light source was 80 W high-pressure Hg lamp located about 5 cm above the head of reactor. UV cutter was used to eliminate UV radiation of Hg lamp and get the higher wavelengths than 420 nm (with wavelength of 420–580 nm). Schematic of the experimental setup was depicted in Fig. 1.

Modified TiO_2 powder (0.07 g) was dispersed inside the Pyrex glass reactor. A feed mixture made from 1,000 ppm acetaldehyde in the air was continuously entered the reactor with a specific flow rate of 15 ml min^{-1} at room conditions, adjusted with mass flow controller, and the outgoing stream was analyzed by gas chromatographic technique. After achieving the steady condition, the source light was turned on. The progress of the reaction was analyzed by detecting acetaldehyde outlet concentration by Gas Chromatograph (VARIAN CP-3800 FID detector GC, column: Propack Q), and the outlet concentration of the acetaldehyde was recorded at steady condition.

Results and discussion

Photocatalytic activity

In order to approximate the photocatalytic activity of the modified samples under visible light irradiation, decomposition of acetaldehyde was studied as an indoor pollution in the continuous stirred reactor. The operational conditions of photocatalytic experiments are listed in Table 2. Figures 2 and 3 show the degradation of acetaldehyde after the light source was turned on using different prepared photocatalysts at the steady conditions. As seen, photocatalytic activities of the modified samples are much higher than P25–TiO_2.

An appropriate amount of doped F atoms might slow down the irradiative recombination process of photogenerated electron and holes in TiO_2 and lead to the formation of new active sites. Also, doping F leads to the enhancement of surface acidity (Li et al. 2005a, b). This would increase acetaldehyde adsorptivity and cause enhancement of the photocatalytic activity. The activity was increased to a maximum with 0.3 F/Ti ratio, whereas further increase in fluoride concentration reduced the activity. It is concluded that high content of fluorine diminishes the surface hydroxyl of TiO_2 (=Ti–OH) and decreases the ability of trapping the electrons; therefore, the photocatalytic activity is stepped down.

It was revealed that annealing TiO_2 powder under NH_4OH/N_2 flow produced visible light-active photocatalysts, and it is concluded that the visible light activities of N-doped TiO_2 are attributed to the significant shifts of the absorption shoulders for their optical absorbance spectra at

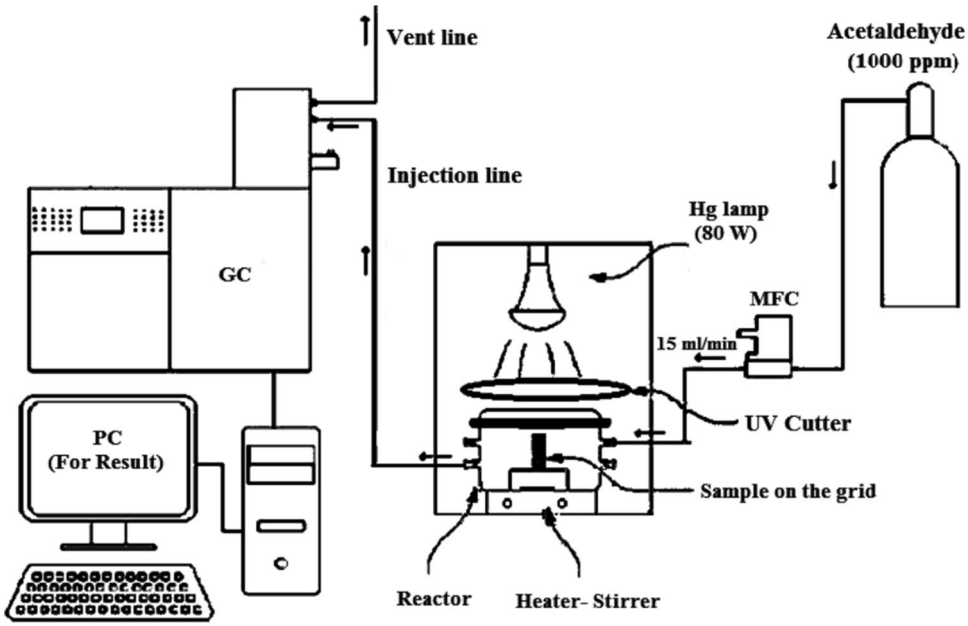

Fig. 1 Experimental setup of the photocatalytic reactor

Table 2 The operation conditions for photocatalytic activity

Temperature	25 °C
Volume of reactor	198 ml
Flow rate	15 ml min^{-1}
Inlet concentration	1000 ppm
Light source	80 W Hg lamp
Amount of catalyst	0.07 g

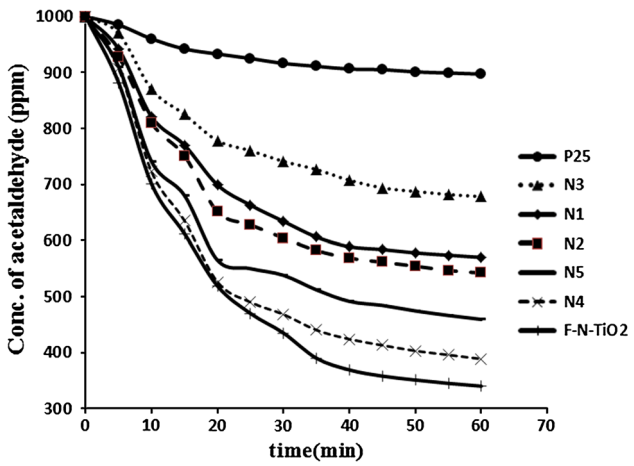

Fig. 2 Photocatalytic activity of P25, N-doped TiO_2, and F–N–TiO_2 samples in continuous reactor

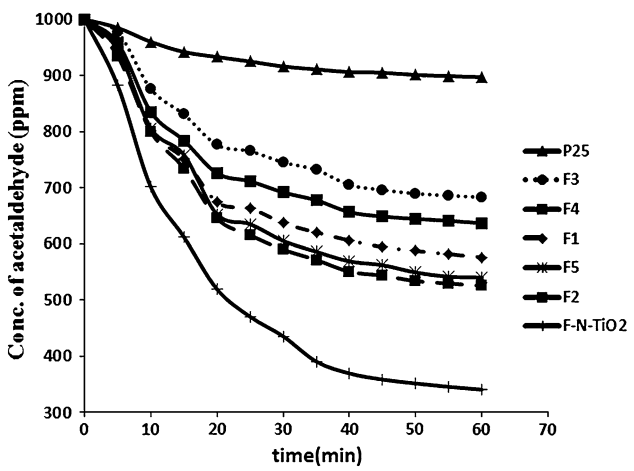

Fig. 3 Photocatalytic activity of P25, F-doped TiO_2, and F–N–TiO_2 samples in continuous reactor

wavelengths between 400 and 550 nm, which was due to the substitutional nitrogen existing in the products. The photocatalytic activities of the N-doped TiO_2 powders gradually decreased with increasing annealing temperature, and sample N4 approached to the best performance among the other samples. Reduction in photocatalytic activities of N-doped TiO_2 samples with annealing temperature might be according to considerable increase in the amount of oxygen vacancy with annealing temperature, because the oxygen vacancies acted as recombination centers for holes and electrons (Liu et al. 2006). Also with increasing temperature, the specific surface area was decreased, therefore resulting in lower photocatalytic activity. The impact of (N_2) carrier gas flow rate shows that higher flow rates cause decreasing residence time of NH_4OH and as a result the number of oxygen substitution with nitrogen atoms steps down, in TiO_2 structure.

As shown in Figs. 2 and 3, F–N–TiO_2 has exhibited the highest activity than the other samples. Due to the synergy effect between N- and F-doped TiO_2, such as low band gap, shift of the absorption spectra into visible region, and formation of new active sites, F–N–TiO_2 powder presented much better photocatalytic performance in photocatalytic degradation of acetaldehyde under visible light irradiation.

XRD analysis

Figure 4 shows the XRD patterns of P25, F2, N4 samples, and F–N–TiO_2 sample. Nitrogen and fluorine peaks are not detected in the samples because of the low doping contents of nitrogen and fluorine; in addition, it would be due to possibly high dispersion of those elements in TiO_2 structure. The average crystallite size of the synthesized TiO_2 was calculated from the XRD data according to Scherer's equation (Carp et al. 2004):

$$d = \frac{k\lambda}{\beta \cos\theta}, \quad (1)$$

where d is the crystallite size, k is a constant (0.9), λ is the wavelength of X-ray (Cu Kα), β is the half-peak width in radians, and θ is the Bragg's diffraction angle in degree. The phase content of a sample was calculated from the integrated intensities of the anatase, rutile, and brookite peaks. If a sample contains only anatase and rutile, the weight fraction of rutile (W_R) could be calculated from:

$$W_R = \frac{A_R}{A_R + 0.884A_A}, \quad (2)$$

where A_A represents the integrated intensity of the anatase (101) peak and A_R is the integrated intensity of rutile (110) peak.

Crystallite size and weight percentage of the crystalline phases of the samples were calculated from the XRD patterns and are listed in Table 3. The crystallite size of F2 and F–N–TiO_2 is larger than that of other samples, indicating that NH_4F improves the growth of F2 and F–N–TiO_2 grains. In order to confirm the result, BET results of the samples are shown in Table 4. F2 and F–N–TiO_2 samples have less specific surface area, in which it confirms that NH_4F improves the growth of F2 and F–N–TiO_2 crystals.

There is not observed any changes in d-space of (101) planes, in the samples, which indicates that samples

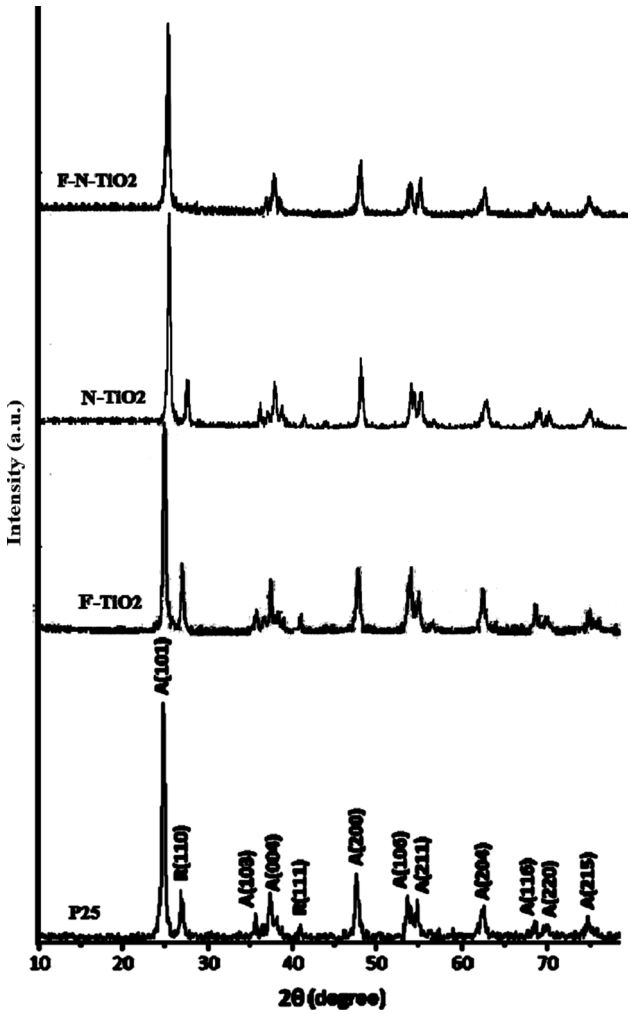

Fig. 4 XRD patterns of P25, F2, N4, and F–N–TiO_2 samples

Table 3 Properties of the sample calculated from XRD patterns

Samples	Crystallite size (nm)	Anatase (wt%)	Rutile (wt%)	*d*-Spacing for (101) plane (Å)
P25	25	80	20	3.52
F2	27	72	28	3.52
N4	24	74	26	3.50
F–N–TiO_2	31	100	–	3.52

possess similar crystallinity and that N and F are incorporated into the lattice without changing the average dimension of the unit cell (Sathish et al. 2005).

FT-IR analysis

As shown in Fig. 5, the FT-IR spectra reveal that all the TiO_2 samples display absorbance bands around 3445, 2365, 1620, and 665 cm^{-1}. The band at 3,445 cm^{-1} corresponds to the

Table 4 Surface area and pore volumes of the samples

Samples	BET surface area (m^2 g^{-1})	Total pore volume (cm^3 g^{-1})	Pore size (Å)
P25	55	0.06	38
F2	52	0.126	114
N4	57	0.058	33
F–N–TiO_2	45	0.087	96

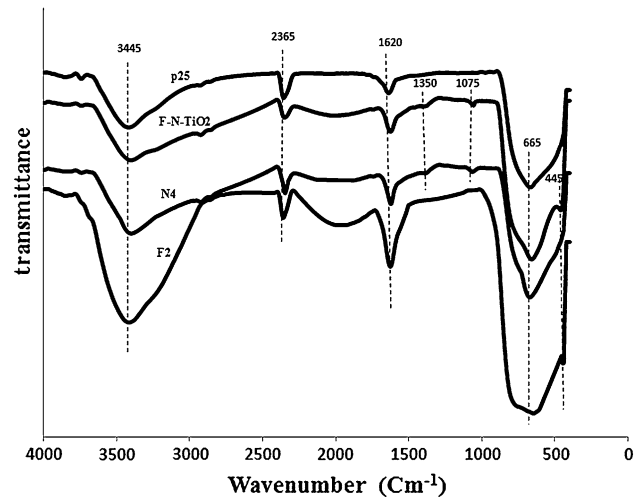

Fig. 5 FT-IR spectra of P25, F2, N4, and F–N–TiO_2 powders

O–H stretching vibration, while the band at 1,620 cm^{-1} results from O–H bending of adsorbed water molecules (Wei et al. 2008; Soler-Illia et al. 2002). The band at 665 cm^{-1} attributed to Ti–O stretching and Ti–O–Ti stretching modes (Huang et al. 2007). The absorption peak at 2,365 cm^{-1} is characteristic of surface-adsorbed CO_2 (Li et al. 2008).

In comparison with P25 powder, N4 and F–N–TiO_2 display additional two absorbance peaks. The peak around 1,075 cm^{-1} can be assigned to the vibration of the N–Ti bond, while the peak at 1,350 cm^{-1} is resulted from the vibration of surface-adsorbed NH_3 (Huo et al. 2009; Sakthivel et al. 2004). Compared to P25, appearance of a new absorption peak at 445 cm^{-1} for F2 and F–N–TiO_2 is indicating the vibration of the F–Ti bond (Ignateva et al. 2004; Nakamoto 1970). The appearance of the N–Ti and F–Ti bonds suggests the incorporation of N and F atoms into the TiO_2 crystal lattice.

Results of DRS

The light absorption characteristics of TiO_2 are changed after doping. The DRS of samples are used to assess the absorption and the band structure of the photocatalyst in UV–Vis region.

As shown in Fig. 6, fluorination influenced the light absorption characteristics. Compared with P25, F2 sample revealed a stronger light absorption in the UV range with a slight shift to the visible range. The absorption spectra of N4 and F–N–TiO_2 were extended into the visible region. For N4 and F–N–TiO_2, a new absorption band was observed in the visible range of 400–550 nm in addition to fundamental absorption edge of TiO_2. The new absorption bands were attributed to the doped N atoms (Asahi et al. 2001; Irie et al. 2003; Li et al. 2005a, b).

The band gap of the samples can be estimated from the tangent line in the plot of the square root of the Kubelka–Munk functions against the photon energy (Kim et al. 1993). The tangent line, which was extrapolated to $[F(R)\cdot h\nu]^{1/2} = 0$, indicated the band gaps of these samples, as shown in Fig. 7, where $F(R) = (1 - R)^2/2R$.

The absorption edge of the samples can be determined from the following equation:

$$E_g = \frac{1,239.8}{\lambda}, \tag{3}$$

where E_g is the band gap (eV) and λ (nm) is the optical absorption edge. The absorption edges and the band gaps of those samples were summarized in Table 5.

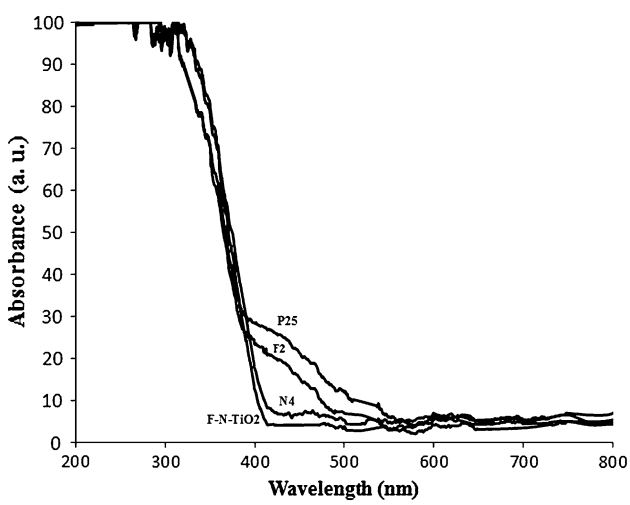

Fig. 6 UV–Vis absorption spectra of P25, F2, N4, and F–N–TiO_2 samples

Table 5 The band gap of the samples

Samples	Band gap (ev)	Absorption edge (nm)
P25	3.15	393
F2	3.09	401
N4	2.92	424
F–N–TiO_2	2.87	432

Kinetic analysis

Many researchers have studied the kinetics of the photocatalytic decomposition of various organic compounds over TiO_2 illuminated and found that all the investigated reactions obey a Langmuir equation (Matthews 1988; Mozzanega et al. 1979). When the photocatalytic reaction obeys a Langmuir model, the relationship between the reaction rate r (μmol g^{-1} min^{-1}) and the acetaldehyde concentration C (μmol l^{-1}) is given as:

$$r = \frac{kK_A C}{1 + K_A C}, \tag{4}$$

where k is the kinetic constant (μmol g^{-1} min^{-1}) and K_A is the adsorption constant (l μmol^{-1}).

In this work, the reaction intermediates and products have not been influenced, significantly; therefore, they have not been detected in Eq. (4).

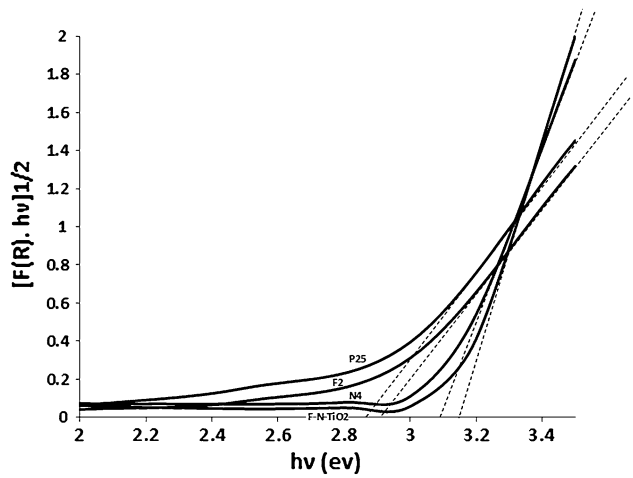

Fig. 7 Kubelka–Munk plot for band gap estimate of the samples

Table 6 The kinetic parameters of different samples under 80 W visible light ($\lambda > 420$ nm)

Samples	k (μmol g^{-1} min^{-1})	K_A (l μmol^{-1})	R^2
P25	3.919	0.0074	0.9477
N1	10.596	0.0203	0.9150
N2	11.305	0.0213	0.9267
N3	8.030	0.0166	0.9473
N4	15.322	0.0273	0.9097
N5	13.074	0.0255	0.9469
F1	10.424	0.0205	0.9600
F2	11.346	0.0231	0.9229
F3	8.093	0.0162	0.9237
F4	9.086	0.0185	0.9582
F5	11.040	0.0223	0.9286
F–N–TiO_2	16.43	0.0321	0.9614

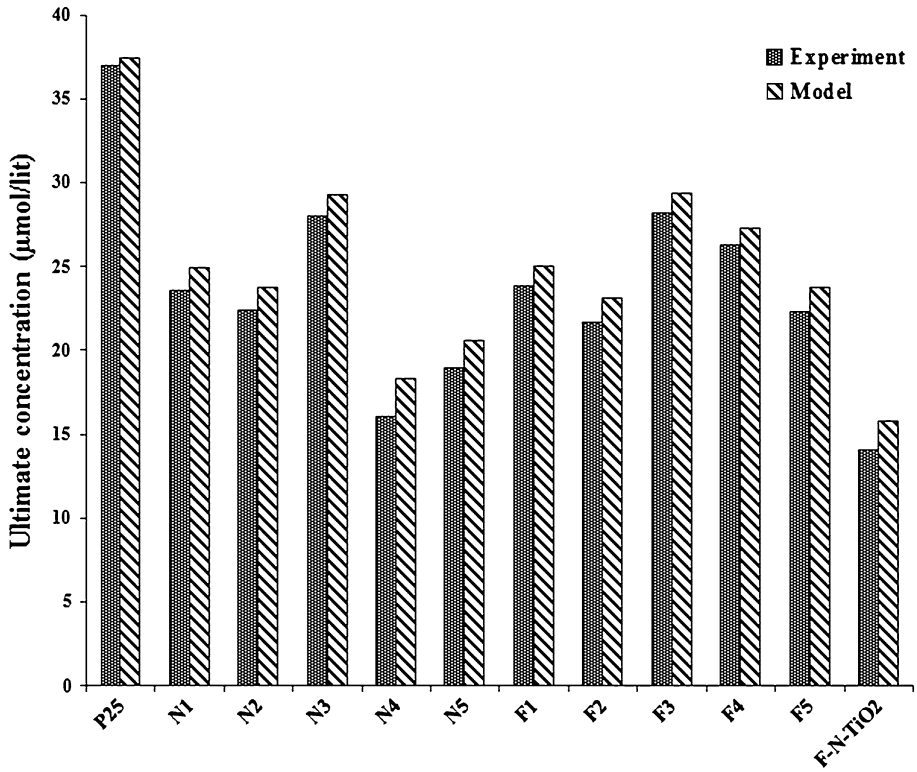

Fig. 8 Comparison between experimental and model predicted in steady state. According to laboratory temperature and pressure: 1 μmol l^{-1} = 24.2 ppm

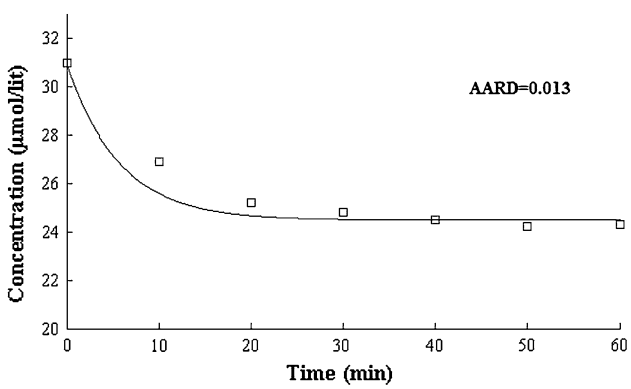

Fig. 9 Validation of the kinetic model parameters for F4 sample at different concentrations and flow rates (750 ppm and 30 ml min^{-1}). The *solid lines* show the calculated values

Writing the material balance for the continuous stirred reactor at unsteady conditions with the assumption of isothermal conditions, complete mixing of the reactor, ignored internal diffusion resistance, and no change in flow rate, the mass balance equation inside the reactor would become as follows:

$$QC_0 - QC - \frac{kK_A C}{1 + K_A C} W = V \frac{dC}{dt}, \quad (5)$$

where Q is the volumetric flow rate (l min^{-1}), W is the weight of catalyst (g), V is the volume of the reactor (l), and t is the time of experiment (min).

To predict kinetic parameters (k, K_A), the direct search method of Nelder–Mead was used by computer programming in MATLAB by minimization of the difference between the model and experimental outlet concentration results as the following objective function:

$$SSRE = \sum \left(1 - \left(C_{\exp eriment}/C_{calculation}\right)\right)^2. \quad (6)$$

According to Eq. (6), kinetic parameters are predicted and shown in Table 6. An agreement between the model and experimental points is shown in Fig. 8.

In order to verify the kinetic model parameters, additional experiment was performed on F4 sample at another concentrations and flow rates (750 ppm and 30 ml min^{-1}). As shown in Fig. 9, the results of the model are in a good agreement with experimental results.

Conclusions

F-doped, N-doped, and F–N–TiO_2 catalysts were successfully synthesized by impregnation, thermal treatment, and sol–gel methods, respectively. N-doped TiO_2 powders were prepared by annealing under NH_4OH/N_2 flow at 400, 500, and 600 °C. F-doped TiO_2 was synthesized with different mass ratios of NH_4F to TiO_2. The results show influential impact of NH_4F amount and temperature on the structure and photocatalytic activity.Due to the synergy effect between doped N and F, such as low band gap, shift

of the absorption spectra into visible region, and formation of new active sites, F–N–TiO_2 possessed the highest photocatalytic activity, and this product degraded 66 % of 1,000 ppm acetaldehyde in 15 ml min^{-1} flow rate in a continuous reactor under 80 W visible light irradiation. The kinetic model was defined as the Langmuir-type equation, and the kinetic parameters were predicted by fitting the dynamic outlet results between model and experiment for all kinds of the fabricated photocatalyst under visible irradiation. The developed kinetic model can be used to design and scale up the photocatalytic reactors under visible light scattering at room conditions.

References

Asahi R, Morikawa T, Ohwaki T, Aoki K, Taga Y (2001) Visible-light photocatalysis in nitrogen-doped titanium oxides. Science 293:269–271

Burda C, Lou Y, Chen X, Samia ACS, Stout J, Gole J (2003) Enhanced nitrogen doping in TiO_2 nanoparticles. Nano Lett 3:1049–1051

Carey JH, Lawrence J, Tosine HM (1976) Photodechlorination of PCB's in the presence of titanium dioxide in aqueous suspensions. Bull Environ Contam Toxicol 16:663–668

Carp O, Huisman CL, Reller A (2004) Photoinduced reactivity of titanium dioxide. Prog Solid State Chem 32:33–177

Fujishima A, Rao TN, Tryk DA (2000) Titanium dioxide photocatalysis. J Photochem Photobiol C 1:1–21

Hattori A, Shimota K, Tada H, Ito S (1999) Photoreactivity of sol–gel TiO_2 films formed on soda-lime glass substrates: effect of SiO_2 underlayer containing fluorine. Langmuir 15:5422–5425

Huang D, Liao S, Quan S, Liu L, He Z, Wan J, Zhou W (2007) Preparation of anatase F doped TiO_2 sol and its performance for photodegradation of formaldehyde. J Mater Sci 42:8193–8202

Huo YN, Bian ZF, Zhang XY, Jin Y, Li HX (2009) Template synthesis of hierarchical Bi_2E_3 (E = S, Se, Te) core–shell microspheres and their electrochemical and photoresponsive properties. J Phys Chem C 113:18075–18081

Ignateva LN, Polishchuk SA, Antokhina TF, Buznik VM (2004) IR spectroscopic study of the structure of glasses based on titanium oxyfluoride. Glass Phys Chem 30:139–141

Irie H, Watanabe Y, Hashimoto K (2003) Nitrogen-concentration dependence on photocatalytic activity of TiO_{2-x} N × powders. J Phys Chem B 107:5483–5486

Joung S, Amemiya T, Murabayashi M, Itoh K (2006) Mechanistic studies of the photocatalytic oxidation of trichloroethylene with visible-light-driven N-doped TiO_2 catalysts. Chem Eur J 12:5526–5534

Kim YI, Atherton SJ, Brigham ES, Mallouk TE (1993) Sensitized layered metal oxide semiconductor particles for photochemical hydrogen evolution from non-sacrificial electron donors. J Phys Chem 97:11802–11810

Klosek S, Raftery D (2001) Visible light driven V-doped TiO_2 photocatalyst and its photooxidation of ethanol. J Phys Chem B 105:2815–2819

Le HA, Linh LT, Chin S, Jurng J (2012) Photocatalytic degradation of methylene blue by a combination of TiO_2–anatase and coconut shell activated carbon. Powder Technol 225:167–175

Li X, Li F, Yang C, Ge W (2001) Photocatalytic activity of WO_x–TiO_2 under visible light irradiation. J Photochem Photobiol A 141:209–217

Li D, Ohashi N, Hishita S, Kolodiazhnyi T, Haneda H (2005a) Origin of visible-light-driven photocatalysis: a comparative study on N/F-doped and N–F-codoped TiO_2 powders by means of experimental characterizations and theoretical calculations. J Solid State Chem 178:3293–3302

Li D, Haneda H, Hishita S, Ohashi N, Labhsetwar NK (2005b) Fluorine-doped TiO_2 powders prepared by spray pyrolysis and their improved photocatalytic activity for decomposition of gas-phase acetaldehyde. J Fluor Chem 126:69–77

Li G, Chen L, Dimitrijevic NM, Gray KA (2008) Visible light photocatalytic properties of anion-doped TiO_2 materials prepared from a molecular titanium precursor. Chem Phys Lett 451:75–79

Li X, Chen Z, Shi Y, Liu Y (2011) Preparation of N, Fe co-doped TiO_2 with visible light response. Powder Technol 207:165–169

Linsebigler AL, Lu G, Yates JT (1995) Photocatalysis on TiO_2 surfaces: principles, mechanisms and selected results. J Chem Rev 95:735–758

Liu S, Chen X, Chen X (2006) Preparation of N-doped visible-light response nanosize TiO_2 photocatalyst using the acid-catalyzed hydrolysis method. Chin J Catal 27:697–702

Matthews RW (1988) Kinetics of photocatalytic oxidation of organic solutes over titanium dioxide. J Catal 111:264–272

Mills A, Hunte SL (1997) An overview of semiconductor photocatalysis. J Photochem Photobiol A 108:1–35

Mozzanega H, Herrmann JM, Pichat P (1979) NH_3 oxidation over UV-irradiated TiO_2 at room temperature. J Phys Chem 83:2251–2255

Nakamoto K (1970) Infrared spectra of inorganic and coordination compounds. Wiley, New York

Sakthivel S, Janczarek M, Kisch H (2004) Visible light activity and photoelectrochemical properties of nitrogen-doped TiO_2. J Phys Chem B 108:19384–19387

Sathish M, Viswanathan B, Viswanath RP, Gopinath CS (2005) Synthesis, characterization, electronic structure, and photocatalytic activity of nitrogen-doped TiO_2 nanocatalyst. Chem Mater 17:6349–6353

Soler-Illia GJAA, Louis A, Sanchez C (2002) Synthesis and characterization of mesostructured titania-based materials through evaporation-induced self-assembly. Chem Mater 14:750–759

Umebayashi T, Yamake T, Itoh H, Asai K (2002) Band gap narrowing of titanium dioxide by sulfur doping. Appl Phys Lett 81:454–456

Wei F, Ni L, Cui P (2008) Preparation and characterization of N–S-codoped TiO_2 photocatalyst and its photocatalytic activity. J Hazard Mater 156:135–140

Wu JCS, Chen CH (2004) A visible-light response vanadium-doped titania nanocatalyst by sol–gel method. J Photochem Photobiol A 163:509–515

Yin S, Yamaki H, Komatsu M, Zhang Q, Wang J, Tang Q, Saito F, Sato T (2003) Preparation of nitrogen-doped titania with high visible light induced photocatalytic activity by mechanochemical reaction of titania and hexamethylenetetramine. J Mater Chem 13:2996–3001

Yu JG, Yu JC, Cheng B, Hark SK, Iu K (2003) The effect of F^--doping and temperature on the structural and textural evolution of mesoporous TiO_2 powders. J Solid State Chem 174:372–380